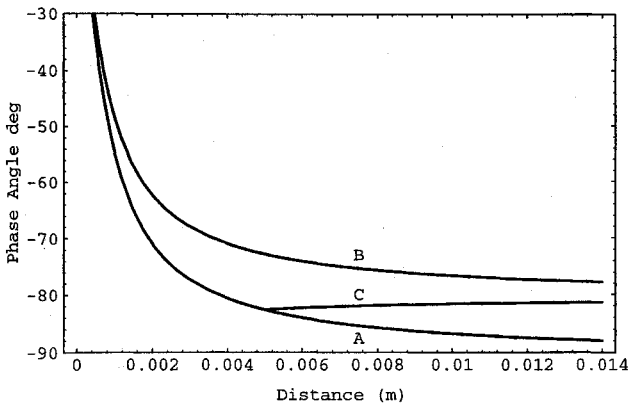


**Fig. 2 Phase angle of the velocity oscillation as a function of distance above the propellant surface for three values of the real part of the distributed combustion response: A, 0.0; B, 10.0 starting at the propellant surface; and C, 10.0 starting at 5 mm above the surface.**

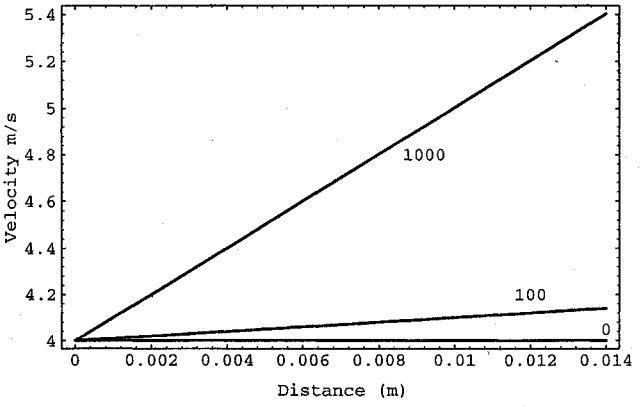


**Fig. 3 Gas velocity as a function of distance above the propellant surface for three values of the volumetric mass release rate caused from distributed combustion.**

a velocity node. Therefore, one can obtain the pressure-coupled distributed combustion response without any experimental ambiguity being introduced by the velocity-coupled response; the disadvantage is that no information on the velocity-coupled distributed combustion response would be obtained. Since the spatial resolution of a magnetic flowmeter is given by the electrode diameter (0.5 mm), the analysis shows that a magnetic flowmeter burner can measure the magnitude and location of the real part of the pressure-coupled distributed combustion response.

The steady-state equations can also be used to study the effect of the steady-state distributed combustion on the flow within the burner. Figure 3 shows the effect of three values for the steady-state volumetric mass release rate resulting from distributed combustion (0, 100, and 1000 kg/m$^3$ s) on the mean gas velocity above the propellant surface. The volumetric mass release caused from distributed combustion causes an increase in the mean gas velocity, which is large enough to be measured by a magnetic flowmeter, thus allowing the determination of the location and magnitude of the steady-state distributed combustion. If one assumes that the products of distributed combustion consist of condensed phases only with the result that heat addition is the only source in the governing equations, similar effects for both the steady and unsteady flowfields are found.

## References

[1]Beckstead, M. W., "Evidences for Distributed Combustion," *24th JANNAF Combustion Meeting*, Vol. 1 (Monterey, CA), Chemical Propulsion Information Agency, Columbia, MD, 1987, pp. 1–12.

[2]Brooks, K. P., and Beckstead, M. W., "Dynamics of Aluminum Combustion," *Journal of Propulsion and Power*, Vol. 11, No. 4, 1995, pp. 769–780.

[3]Wilson, J. R., and Micci, M. M., "Direct Measurement of High Frequency, Solid Propellant, Pressure-Coupled Admittances," *Journal of Propulsion and Power*, Vol. 3, No. 4, 1987, pp. 296–302.

[4]Cauty, F., Comas, P., Vuillot, F., and Micci, M. M., "Magnetic Flow Meter Measurement of Solid Propellant Pressure-Coupled Responses Using an Acoustic Analysis," *Journal of Propulsion and Power*, Vol. 12, No. 2, 1996, pp. 436–438.

[5]Culick, F. E. C., "The Stability of One-Dimensional Motions in a Rocket Motor," *Combustion Science and Technology*, Vol. 7, No. 4, 1973, pp. 165–175.

[6]Micci, M. M., Caveny, L. H., and Sirignano, W. A., "Linear Analysis of Forced Longitudinal Waves in Rocket Motor Chambers," *AIAA Journal*, Vol. 19, No. 2, 1981, pp. 198–204.

# Impulse Function and Drag in Scramjet Inlet Models

Takeshi Kanda,* Kouichiro Tani,*
Tomoyuki Komuro,† Atsuo Murakami,†
Kenji Kudo,† and Nobuo Chinzei‡
*National Aerospace Laboratory, Miyagi 981-15, Japan*

## Introduction

In a typical airframe-integrated scramjet, for example, the NASA Langley-type scramjet, the side walls in the inlet function as a compression system. The inlet has a bottomless geometry, and sometimes has a swept angle to guarantee startability. The open bottom results in spillage and the swept angle increases it. To discuss engine performances, appropriate estimation of drags in such an inlet, including the spillage of mass and momentum, is required.

The shock-wave relation can be applied to analyze the airflow in the inlet. However, estimation based on this relation does not include the end effect of the wall or the open bottom. Furthermore, when the inflow Mach number is low, or the swept angle is large, the velocity component, which the shock-wave relation is applied to, becomes subsonic.[1] To date, there have been relatively few experiments and numerical simulations investigating the characteristics of the inlet drag and those of the spilled air, and consequently, there are few reports dealing with these characteristics.[2–4]

In the present study, several kinds of side-wall compression-type inlets were tested, and the impulse function and the drag in the inlet models with spillage were investigated.

## Experimental Apparatus

A blow-down-type Mach 4.1 wind tunnel was used in the present testing.[1] The total pressure and the total temperature of the working fluid, air, were 1.6 MPa, and 290 K, respec-

Received Oct. 5, 1995; revision received June 4, 1996; accepted for publication June 4, 1996. 

*Senior Researcher, Kakuda Research Center, Ramjet Propulsion Research Division, Kimigaya, Kakuda. Member AIAA.

†Senior Researcher, Kakuda Research Center, Ramjet Propulsion Research Division, Kimigaya, Kakuda.

‡Head, Ramjet Performance Section, Kakuda Research Center, Ramjet Propulsion Research Division, Kimigaya, Kakuda. Member AIAA.

**Table 1 Inlet model side-wall geometry**

| Model | A | B | C | D | E | F |
|---|---|---|---|---|---|---|
| Swept angle, $\alpha$, deg | 45 | 60 | 30 | 0 | 45 | 45 |
| Contraction ratio, $w_{in}/w_{c,in}$ | 5 | 5 | 5 | 5 | 3 | 7 |

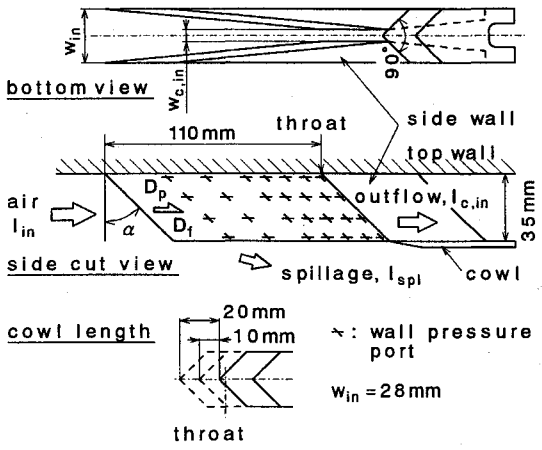


**Fig. 1 Inlet model.**

tively. The unit Reynolds number was $6 \times 10^7$ m$^{-1}$. The inlet model shown in Fig. 1 was attached to the wall of the wind tunnel. The height of the boundary layer at 99% of the free-stream velocity was 10 mm at the entrance of the model. Six kinds of side walls (Table 1) and the three kinds of cowls were used for a total of 18 models. The cowls were named 0, 10, and 20 after the length from the throat to the tip of the cowl (Fig. 1).

Wall pressure was measured at 28 points on one of the side walls, as shown in Fig. 1, and the pitot pressure was measured at 35 points at the throat: at seven different positions from the top wall and at five different positions from the side wall.[1] Because measuring static pressure is very difficult, the wall pressure at the throat was used to obtain the flow properties from the pitot pressure. The pressure drag was calculated from the wall pressure, and the impulse function of the outflow was calculated from the pitot pressure and the wall pressure at the throat.

The wall pressure was different from the static pressure up to 50% at the throat according to the calculated results by the shock-wave relation. This resulted in 20% error in the mass flow rate and 13% error in the impulse function at the throat.

## Impulse Function and Drag

The net engine thrust $F_{net}$ is expressed with the impulse function $I$ as follows:

$$F_{net} = I_{exit} - I_{in} + I_{spl} \tag{1}$$

The subscripts exit, in, and spl indicate the engine exit, engine entrance, and the spillage, respectively. The cross section of the stream tube of the inflow air is equal to the projected geometrical cross section of the inlet at the engine entrance, and there is no influence of the spillage on the impulse function or on the mass flow rate at the engine entrance. When the engine thrust is estimated, the spilled impulse function, as well as the impulse functions of the inflow air and the exhaust gas, must be evaluated.

A schematic diagram of the impulse function and the drag in the inlet is shown in Fig. 1. $D_p$, $D_f$, and $I_{c,in}$ are, respectively, the pressure drag, the friction drag of the inlet, and the impulse function at the combustor entrance. The conservation of momentum is expressed as

$$I_{in} = I_{c,in} + D_f + D_p + I_{spl} \tag{2}$$

The friction coefficient was estimated at about 0.003 on the inlet wall in the present test conditions with the formula of van Driest.[5] The estimated value of the friction drag of the inlet was about 3 N, whereas that of the pressure drag was 20 N. The friction drag was neglected in the present study because of its value being smaller than that of the pressure drag, and the difficulty of measuring it. The spilled impulse function was calculated with Eq. (2).

## Results and Discussion

Figure 2 shows the ratios of the impulse functions and the drag. They are nondimensionalized with the impulse function of the incoming air. The explanation of the symbols is as follows: 45-5(10) stands for the model with a swept angle of 45 deg, a contraction ratio of 5, and a 10-mm cowl.

As shown in Fig. 2, the ratio of the impulse function of the spilled air was larger than that of the mass flow rate of the spilled air in several models. It can be seen that there was a contradiction, namely, the spilled air had a larger stream thrust function than the inflow air. The stream thrust function $Sa$ is the proportion rate between impulse function and mass flow rate[6]:

$$Sa = I/\dot{m}$$

$$= u + (P \cdot A)/\dot{m} \tag{3a}$$

$$Sa = \sqrt{\frac{R \cdot T0}{\gamma}} \frac{1 + \gamma M^2}{M\sqrt{1 + (\gamma - 1)M^2/2}} \tag{3b}$$

Error caused by the usage of wall pressure would have scattered the test results. The contradiction was caused by other reasons, for example, overestimation of the mass flow rate in the region between the wall and the pitot pressure measuring points at the throat. The error caused from overestimation was up to 0.1 in the captured mass flow rate. It caused a large error in the range of the small spilled airflow rate. The overestimation caused 0.3 to appear as 0.23 of the ratio of the mass flow rate of the spilled air. On the other hand, the impulse function was relatively unaffected by the decrease in velocity near the wall because the pressure term, $P \cdot A$, as well as the velocity term, $u \cdot \dot{m}$, contributed to the impulse function [see Eq. (3a)]. Therefore, when the spilled airflow rate was small, and the inflow air was decelerated, the stream thrust function of the spilled air appeared to be larger than that of the inflow in the figure because of the large error in mass flow rate coupled with the small error in impulse function.

The spilled impulse function was proportional to the spilled air mass flow rate, even in the unstarting condition. The ratio of the stream thrust function of the spilled air to that of the inflow air $Sa_{spl}/Sa_{in}$ was 0.85 as shown in Fig. 2. In consideration of the previously mentioned error, the stream thrust function of the spilled air was almost equal to that of the inflow

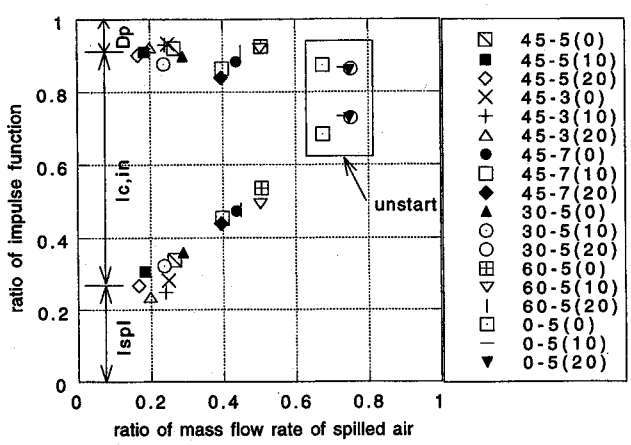


**Fig. 2 Ratio of impulse function and drag.**

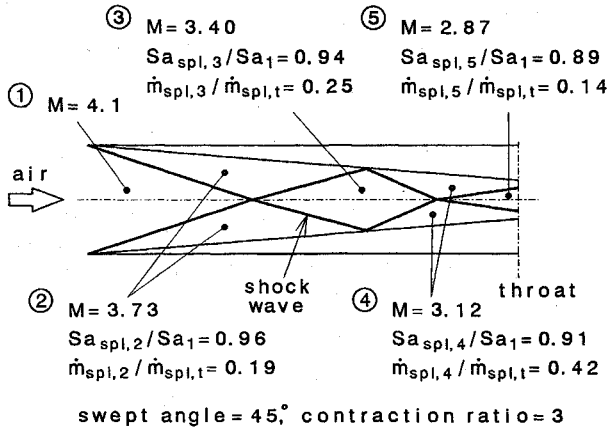


**Fig. 3 Stream thrust function in the inlet using the shock-wave relation.**

air. The stream thrust function does not change very much with Mach number [see Eq. (3b)]. For example, when a Mach number changes from 10 to 3, the stream thrust function decreases to 0.88 of that of the Mach number of 10. In the preliminary estimation of the engine thrust, the stream thrust function of the spilled air can be estimated as being equal to that of the inflow air. According to the results by Voland,[1] the ratio of the stream thrust function of the spilled air to that of the inflow air was 0.9, and was also around unity.

Figure 3 shows the change of the stream thrust function in the two-dimensional flow of one of the inlets, 45-3(0), calculated using the shock-wave relation. The shock-wave relation was applied to the plane perpendicular to the leading edge of the side wall. The spillage was calculated using the downward component of the velocity and the density after the shock wave, and the area of the specified section. $\dot{m}_{spl,t}$ is the total flow rate of the spilled air. $Sa_{spl,i}$ is the stream thrust function of the spilled air from section $i$. It does not have the pressure contribution of the second term in Eq. (3a), because the bottom of the side wall was parallel and the plane of the spillage was also parallel to the direction of thrust or drag. The stream thrust function did not change very much near the throat.

As shown in Fig. 2, there was no large change in the pressure drag of the inlet throughout the testing, regardless of whether or not the inlet was in the starting condition. The pressure drag did not increase with the contraction ratio to the degree predicted by the shock-wave relation. The ratio of the spilled air was 0.15 in Fig. 3, while it was 0.25 in the testing. The ratios of the pressure drag, spilled impulse function, and the impulse function of the outflow to the impulse function of the inflow air were 0.10, 0.14, and 0.76, respectively, whereas those in the testing were 0.07, 0.28, and 0.65, respectively. The difference was caused by the spillage caused by the pressure difference between inside and outside the inlet, and because of the end effect of the wall. The pressure difference induces spillage of the downward flow. For example, there is spillage even in the model with no swept angle. Around the top wall, the shock wave from the leading edge of the side wall was rather conical, and the pressure increase across the shock wave was smaller than across the plane shock wave. The disagreement of the calculated values with the experimental results shows the limitation of application of the shock-wave relation for estimation of the drags in the inlet.

## Conclusions

The impulse functions and the drag of the side wall compression-type scramjet inlet models were investigated in a Mach 4 flowfield. The following points were clarified:

1) The stream thrust function of the spilled air from the inlet was almost equal to that of the incoming air, and did not change so much with the decrease of the Mach number.

2) The pressure drag of the inlets showed little change, regardless of the model geometry, and regardless of whether or not the inlet was in the starting condition.

## Acknowledgment

The authors thank Goro Masuya of Tohoku University for useful discussions.

## References

[1]Kanda, T., Komuro, T., Masuya, G., Kudo, K., Murakami, A., Tani, K., Wakamatsu, Y., and Chinzei, N., "Mach 4 Testing of Scramjet Inlet Models," AIAA Paper 89-2680, July 1989.

[2]Voland, R. T., "Methods for Determining the Internal Thrust of Scramjet Engine Modules from Experimental Data," AIAA Paper 90-2340, July 1990.

[3]Vinogradov, V. A., and Stepanov, V. A., "Numerical and Experimental Investigation of Airframe-Integrated Inlet for High Velocities," *Journal of Propulsion and Power*, Vol. 8, No. 1, 1992, pp. 151–157.

[4]Kumar, A., Singh, D. J., and Trexler, C. A., "Numerical Study of the Effect of Reverse Sweep on Scramjet Inlet Performance," *Journal of Propulsion and Power*, Vol. 8, No. 3, 1992, pp. 714–720.

[5]White, F. M., "Viscous Fluid Flow," McGraw–Hill, New York, 1974, pp. 632–640.

[6]Heiser, W. H., and Pratt, D. T., *Hypersonic Airbreathing Propulsion*, AIAA Education Series, AIAA, Washington, DC, 1994, p. 63.

# Hollow Projectile Operation in the Ram Accelerator

A. Sasoh,* A. J. Higgins,† C. Knowlen,‡ and A. P. Bruckner§
*University of Washington, Seattle, Washington 98195-2250*

## Introduction

THE ram accelerator is a chemically energized mass driver that has the potential for launching heavy payloads at high speeds.[1] In this device, a subcaliber projectile is injected at supersonic speed into a tube filled with pressurized combustible gas mixtures. Combustion is initiated by the passage of the projectile that results in a pressure field that continuously accelerates it. Applications of this technology include direct space launch, hypersonic ground test facilities, a research tool to study supersonic reactive flow phenomena, and hypervelocity impact experiments. To realize these applications, the operational characteristics of the ram accelerator need to be better understood.

Currently, the experimental diagnostics of the flowfield in a ram accelerator are limited to measurements made at the tube

Received Oct. 4, 1995; revision received May 28, 1996; accepted for publication June 9, 1996. 

*Visiting Scholar, Aerospace and Energetics Research Program; currently Associate Professor, Shock Wave Research Center, Institute of Fluid Science, Tohoku University, 2-1-1 Katahira, Aoba-ku, Sendai 980-77, Japan. Member AIAA.

†Graduate Student, Aerospace and Energetics Research Program. Student Member AIAA.

‡Research Scientist, Aerospace and Energetics Research Program. Member AIAA.

§Professor, Aerospace and Energetics Research Program. Associate Fellow AIAA.